AD-A239 803

UMENTATION PAGE

SBI/NORDA

. Report Date.	3. Report Type and Dates Covered.
June 1991	Contract

(2)

4. Title and Subtitle.

Sea Ice Elastic Moduli: Determination of Biot Parameters Using In-Field Velocity Measurements

5. Funding Numbers.

Program Element No. 63785N
Project No. 0120
Task No. 803
Accession No. DN250128

6. Author(s).

K. L. Williams* and R. E. Francois*

7. Performing Organization Name(s) and Address(es).

Applied Physics Laboratory
University of Washington
Seattle, WA 98105

8. Performing Organization Report Number.

9. Sponsoring/Monitoring Agency Name(s) and Address(es).

Naval Oceanographic and Atmospheric Research Laboratory
Ocean Acoustics and Technology Directorate
Stennis Space Center, MS 39529-5004

10. Sponsoring/Monitoring Agency Report Number.

CR 036:91

11. Supplementary Notes.

Contract N00039-91-C-0072
*Applied Physics Laboratory

12a. Distribution/Availability Statement.

Approved for public release; distribution is unlimited.

12b. Distribution Code

13. Abstract *(Maximum 200 words).*

The elastic moduli of sea ice are determined from high frequency velocity measurements made on small samples extracted from the ice canopy. The experimental apparatus for determining the velocities is described and was designed to allow quick in-field measurement. The experimental procedure included measurement of the ice sample salinity and temperature and the results given here allow prediction of elastic moduli from knowledge of these more easily obtainable physical parameters. The elastic moduli determined are those appropriate for a specialized Biot model in which the ice is viewed as a closed pore isotropic material. With the Biot model put forth here, seven parameters are needed to predict acoustic velocities, all of which are easily interpreted physically and are given here in terms of their salinity and temperature dependances.

139

91-08565

14. Subject Terms.	15. Number of Pages.
Ice, temperature, pressure	33
	16. Price Code.

17. Security Classification of Report.	18. Security Classification of This Page.	19. Security Classification of Abstract.	20. Limitation of Abstract.
Unclassified	Unclassified	Unclassified	SAR

5/31/91

Sea Ice Elastic Moduli: Determination of Biot Parameters using In-Field Velocity Measurements

K. L. Williams, R. E. Francois

Applied Physics Laboratory

College of Ocean and Fisheries Sciences

University of Washington

Seattle, Washington,98105

ABSTRACT

The elastic moduli of sea ice are determined from high frequency velocity measurements made on small samples extracted from the ice canopy. The experimental apparatus for determining the velocities is described and was designed to allow quick in-field measurement. The experimental procedure included measurement of the ice sample salinity and temperature and the results given here allow prediction of elastic moduli from knowledge of these more easily obtainable physical parameters. The elastic moduli determined are those appropriate for a specialized Biot model in which the ice is viewed as a closed pore isotropic material. With the Biot model put forth here, seven parameters are needed to predict acoustic velocities, all of which are easily interpreted physically and are given here in terms of their salinity and temperature dependances.

PACS numbers: 43.20.Bi, 43.20.Hg, 43.30.Ma, 43.35.Cg

I. INTRODUCTION

General prediction and modeling of acoustic propagation in and scattering from the ice canopy requires input of the longitudinal and shear wave velocities in this inhomogeneous material.[1-3] These velocities are well modeled, as will be shown, by invoking constitutive relationships of the elastic moduli to otherwise measurable or predictable properties such as temperature and salinity of the sea ice. These fundamental ice moduli can be established by carefully controlled measurement of the acoustic velocity in sea ice. Three primary velocity measurement techniques have been used in both saline and non-saline ice: seismic and flexural wave measurement[4–6], resonance vibration of ice rods[4,7–9], and propagation of high frequency pulses in ice cores[9–21].

In much of the pulse technique work to date ice cores were taken and allowed to reach equilibrium with the air temperature or were refrigerated and taken to a laboratory for the velocity measurements. The multiphased porous nature of sea ice makes it extremely sensitive to this kind of handling procedure and the *in-situ* equilibrium ratios of the liquid and solid phases as well as the properties of each phase are changed[22]. This correspondingly changes the acoustic behavior, a fact which provides sufficient motivation for design of an acoustic pulse experiment whose goal is to obtain velocities quickly in the field while minimizing the change of the temperature of ice core samples before and within the measurement cycle and maintaining reasonable uncertainties in results. The pulse experiment described in Section II was designed with this goal in mind.

The porous nature of sea ice also makes it a natural candidate for use of Biot theory[23,24] in determining elastic moduli from velocity measurements. Experimentally, the difficulty lies in the need to determine a large number of parameters in the full Biot theory for an anisotropic open pored medium[2]. However, as shown in Section III, if one specializes the theory to examine a closed pore isotropic porous media the number of needed parameters reduce to seven, all of

which are easily interpreted physically and which are amenable to experimental determination. Even with this specialization the results represent a generalization of previous ice models[25].

In the ensuing sections we outline in turn: the procedure, apparatus, and results for an in-field experiment in which the acoustic vertical velocities of sea ice were measured (Section II); development of the relations between velocity and elastic moduli appropriate for a simplified Biot model of sea ice, and the determination of the Biot moduli using the experimental velocity results (Section III); application of the Biot model in examining temperature cycling effects on acoustic velocities, and in calculating average velocities for the ice canopy as a function of thickness and air-ice surface temperature (Section IV). In Section V we summarize.

It is important to stress at the outset that we view the present manuscript not only as a summary of research results but also an introduction of a methodology by which other researchers might obtain velocity data and incorporate their results such as to improve the in-field data base from which the moduli are determined. For this reason we include, as an appendix, a table of our velocity results and plan to document any future measurements which add to the in-field data base via short letters to the editor. As a last introductory comment, a researcher, with temperature and salinity measurements in hand and needing simply a quick prediction of acoustic velocities, may use Eqs.11-14 to determine porosity and then Eqs. 3 and 4 to determine the longitudinal and shear velocities (this quick calculation is restricted to volume fraction porosities less than 0.3).

II. EXPERIMENT

A. Procedure and Apparatus

A first generation experimental design was described in Ref. 1. A preliminary in-field experiment using the design and procedure discussed there led to several changes resulting in the methodology outlined in this section and used to obtain the data to be presented below. The

experiment discussed here was one part of the arctic research carried out at the Applied Physics Laboratory Ice Station (APLIS 90) (established and occupied for a seven week period from the end of February until the middle of April 1990) in the Beaufort Sea.

A 7.6 cm diameter SIPRE corer was used to obtain vertical (i. e., the SIPRE corer was oriented perpendicular to the air-ice interface) ice core samples for measurement. As touched upon in the introduction, a major concern is measurement of acoustic velocities without significant ice core temperature change. Several steps were taken in order to minimize the change of temperature before and during measurement. First, only short lengths (20-30cm) of core were removed and prepared for measurement at one time. As soon as a section was removed a cylindrical foam plug was placed in the resulting hole to minimize down hole cooling. The extracted length was immediately sectioned into 5 to 8 cm lengths using a bandsaw and then placed in fiberglass foam insulation.

Figure 1 diagrams the experimental apparatus used after this initial preparation. The experimental procedure was carried out by two researchers, one outside (ambient temperature -2 to -30°C) focused on core handling and one inside recording all data, coordinating efforts with a portable radio set. In outside operations, one eighth inch diameter holes were drilled from the side to the center of each section with a cordless drill and temperatures recorded with a YSI precision thermistor probe accurate to 0.1° C. Starting with the section furthest from ambient temperature, the time of flight for each wave type and the section length were measured using the velocimeter built in-house and shown in Figure 1.

The time of flight measurements used two "dual wave" longitudinal/shear transducers custom built by Kraukramer Branson with a shear (longitudinal) resonance frequency of about 700 (950) kHz. By far the greatest difficulty is obtaining shear wave coupling between transducer and ice sample. In the laboratory and previous field pilot tests attempts were made to use shear coupling gels without success. Our solution for the present work was to build small removable plastic

dams one of which was placed around the transducer at the bottom of the velocimeter. Fresh water at its freezing temperature was placed in the dam and the saline ice sample placed on top so that a thin layer of water was between transducer and sample. A rubber grommet ("O" ring) was placed on top of the sample to act as another dam, water pored in the center of the grommet, and the upper transducer lowered so that a thin layer of water also existed between this transducer and the sample. The transducer at one end of the velocimeter was excited by a pulser/receiver and the delayed signal was acquired by the receiving transducer, amplified by the same pulser/receiver, and output on a 10 MHz digital scope where it was stored on the built-in disc memory after both longitudinal and shear coupling was established. The longitudinal coupling was always immediately apparent and as the fresh water froze the shear coupling was developed. Shear coupling was not always obtained and as might be expected was most difficult in the higher temperature cores. The results presented here use only those cores in which both longitudinal and shear coupling were obtained. In practice the establishment of shear wave coupling was observed by the inside researcher to occur within a few seconds to a minute depending on the core temperature. A typical waveform is shown in Figure 1.In the waveform the first pulse is the longitudinal wave and the second, much larger pulse is the shear wave.

The velocimeter had a caliper attached with a resolution of 0.001 inch; however, roughness of the section ends lead us to use a more conservative estimate of length uncertainty i.e. 0.01 inch. Two measurements were made on each sample. First, the transducers were brought into contact with the sample without the water dams to get a true length measurement of the sample. Then the shear coupling was established and another length measurement was made. The difference gives the fresh water path length. To determine the time delay due to the fresh water path length we use Eq. 1 and 2 which we have derived from the data of Ref. 10 to get the longitudinal (C^{fr}_{l}) and shear (c^{fr}_{s}) velocities of freshwater ice as a function of temperature. In making the correction, we assume that the fresh water ice reaches temperature equilibrium with the core.

$$c^{fr}_{l} = 3800 - 22.2\,(T + 2) \quad (m/s) \tag{1}$$

$$c^{fr}_{s} = 1810 - 10.8\,T \quad (m/s) \tag{2}$$

for the longitudinal (c^{fr}_{l}) and shear (c^{fr}_{s}) velocities of fresh water ice as a function of temperature (in degrees C). Note that T is negative so that the velocities increase with decreasing T. Dividing the measured path length difference by the computed fresh water velocity gives the fresh water part of the travel time measurement. This eliminates the fresh water part of the delay from the travel time measurements. The total freshwater path length never exceeded 0.5 cm and in most cases was less than 0.3 cm.

The scope was triggered by a sync pulse sent out at the time of sender excitation so that the time of flight is directly measurable. Inherent delay and "zero" sample length were checked beforehand with sender and receiver in direct contact. Time of flight measurements on a calibrated aluminum cylinder allowed elimination of systematic time scale errors.

After the time of flight measurement, the temperature of the core section was again measured and then the sample was placed in a sealed container and allowed to melt. After melting, the section salinity was determined with an accuracy better than 0.01 ppt from conductivity/temperature measurement[26]. Then the temperature of the core (the temperature at the end of the velocity measurement was used since those temperatures were taken within seconds after this measurement) and the salinity were used to calculate both the porosity β and the density ρ of the sample using the equations given in Section III.A below. The calculation of density assumes no air content in the ice core. Comments on this assumption and the possible effects of air in the ice core are given in the summary.

The procedure above was carried out on 89 sections, both longitudinal and shear coupling was attained on 53 of these samples. The porosities and velocities calculated for these sections are given in the appendix. Of the 53 sections, 46 were from cores extracted from the original ice

canopy in the region of the ice camp. The remaining 7 were from cores extracted from refrozen large openings that had been made through the ice canopy for another experiment.

B. Acoustic Velocities and "effective" Moduli

Figure 2 shows the data obtained and least squares curve fits to the data. The curve fits give

$$c_l = 3741(1-1.85\beta)^{1/2} \quad \text{(m/s)} \tag{3}$$

$$c_s = 1839(1-2.79\beta)^{1/2} \quad \text{(m/s).} \tag{4}$$

The porosity β is in volume fraction (see Section III). The functional form of the curve fits to the data were physically motivated by the vertically elongated structure of the brine inclusions[27,28]. If the sea ice is pictured as a fresh water ice matrix with vertically oriented brine inclusion cylinders, and the porosity reduction therefore associated with reduction of the cylinders diameter, then moduli for vertically propagating sound would be proportional to (1-const* β) which in turn implies sound speeds with a $\sqrt{1-\text{const}*\beta}$ dependence.

Reference 1 discusses in some detail the magnitude of uncertainties in individual moduli values. Here we simply point out that the most significant error is in determining porosity from temperature and salinity for temperatures near freezing. The magnitude of typical errors has been indicated by error bars for a few points in Fig. 2.

In preparation for determination of Biot moduli in the next section it is useful to define and determine two "effective" moduli. Previous analyses of sea ice moduli have concentrated on determining Young's modulus and Poisson's ratio. However for comparison with Biot porous solid results it is more natural (see Section III) to determine an effective bulk modulus K^{eff}_i and shear modulus μ^{eff}_i of the ice. These moduli are defined via

$$c_l^2 = (K^{eff}_i + \frac{4\mu^{eff}_i}{3})/\rho \quad (5)$$

$$c_s^2 = \frac{\mu^{eff}_i}{\rho} \quad (6)$$

Using Eqs. 3 through 6 we then have

$$K^{eff}_i = (9.49\times10^6)(1-1.40\beta)\rho \quad (Nt/m^2) \quad (7)$$

$$\mu^{eff}_i = (3.38\times10^6)(1-2.79\beta)\rho \quad (Nt/m^2) \quad (8)$$

where the density is in Kg/m^3. Since the moduli cannot physically have values less than zero these equations must have upper porosity limits of validity. We postpone discussion of porosity limits until the Biot moduli are determined below where extrapolation to high values of porosity will allow a physical check of results. However, in natural sea ice the salinity and temperature at the bottom most porous layer is typically 10 ppt and -2°C respectively and the equations in Section IIIa imply an upper limit of porosity of about 0.25. This value is well within the limits of positive moduli for Eqs. 7 and 8 and furthermore indicates that the porosities obtained in the experiment and shown in Figure 2 span a large fraction of those realizable in the arctic. In the next section these effective moduli will be used to determine Biot moduli.

III. THEORY

In this section equations for calculating porosity and density from salinity and temperature are first summarized (Section IIIa). Next a specialized Biot model is presented (Section IIIb). Finally, the results of Sections IIIa and IIIb are used in conjunction with Eqs. 7 and 8 to determine the Biot moduli of the model (Section IIIc) which then may be used in predictions of acoustic velocities.

A. Calculation of Porosity and Density

We make the assumption that there is no air and neglect salt precipitation in the brine (this assumption is in keeping with the Biot treatment of ice, below, as a two component porous medium), whereupon we can write

$$\rho = \beta\rho_f + (1-\beta)\rho_s \tag{9}$$

where ρ is the bulk density of the ice, ρ_f is the density of the fluid brine, and ρ_s is the density of the fresh water ice making up the solid frame matrix.

Now using Eq. 9, and

$$\beta = \frac{\rho S}{\rho_f S_f} \text{ (From Ref.29)}$$

which is appropriate when salt precipitation is neglected, we can solve for β in terms of the bulk salinity S, fluid brine salinity S_f, and, densities ρ_f and ρ_s,

$$\beta = \frac{\rho_s S}{\rho_f S_f - \rho_f S + \rho_s S}. \tag{11}$$

The temperature dependencies of the densities and brine salinity in Eq. 11 are (from Refs. 22 and 29)

$$\rho_s = 917.0 - 1.403\times10^{-1}\, T \tag{12}$$

$$\rho_f = 1000.0 + 0.8\, S_f(T) \tag{13}$$

$$S_f = -3.9921 - 22.700\, T - 1.0015\, T^2 - 0.19956\, T^3. \tag{14}$$

where the densities are in Kg/m^3, the salinity in ppt, and the temperature in degrees C.

In practice Eqns. 11-14 were used to determine porosity from S and T measurements and then Equation 9 and 12-14 used to determine density.

B. Development of Simplified Biot Model

Reiterating from Section I, the specialization that we use consists of assuming the brine filled pores in the saline ice are sealed and that the ice is isotropic. With this restriction the number of parameters which must be specified is reduced to seven and are easily interpreted. The sealed-pore assumption is most valid away from the skeletal layer at the water/ice interface[28].

The isotropic assumption counterdicts our vertical cylindrical pore picture used in obtaining Eqs. 3 and 4. In reality, with the vertical orientation of the experiment, we are measuring two of the parameters in a full transversely isotropic model of the ice. In particular, if one imposes the closed pore assumption in Ref. 2 and examines plane wave motion in the vertical direction the parameter H introduced below can be associated with the parameter B_4 of Ref. 2 and the parameter μ_b below associated with B_5 of Ref. 2. However, use of the simplified model here affords physical insight not easily obtainable using the full model of Ref. 2. Furthermore, in light of the scarcity of experimental results for acoustic moduli (see discussion in Sec VIIa of Ref.2), use of the simplified model and experimental results presented here to address propagation for directions other than vertical would seem to be a viable alternative to use of a more sophisticated model where parameter measurements are not available at present.

The terminology to be used here mirrors that of Ref. 30. A complete development of Biot's theory may be found in Refs 23, 24, 31, and 32. We simply note here that Biot's examination of propagation of energy through a porous material began with a determination of the potential energy stored within the material and the kinetic energy due to the motion of both the solid and liquid phases. With these he could write the Lagrangian density and determine the equations of motion. From this type of analysis one can derive a set of coupled equations of motion for the liquid and solid. These equations are given as Eq. 6 of Ref. 30 (we note a typographical error in the first of those equations ie 2μ should be replaced by μ). These equations are coupled via the relative motion of the liquid and solid. Assuming a sealed-pore structure eliminates this relative motion. To correctly handle this situation within the context of Biot theory one must really go back to the potential and kinetic energy equations[31,32] and eliminate the relative motion. Doing

so one finds that only one equation survives and is of the form

$$\mu_b \nabla^2\vec{u} + (H-\mu_b)\nabla(\nabla\cdot\vec{u}) = \rho \frac{\partial^2\vec{u}}{\partial^2 t} \tag{15}$$

and ρ is as defined in Eq. 9. In Eq. 15 $\vec{u}$ is a displacement vector for differential volume of the solid, μ_b is the shear modulus of the frame, and H is combination of bulk moduli for the frame, solid, and fluid which is will be given below. If the displacement vector is written as a combination of scalar (ϕ) and vector (ψ) potentials

$$\vec{u} = \nabla\phi + \nabla\times\psi \tag{16}$$

then Eq. 15 can be rewritten as two equations

$$H\nabla^2\phi = \rho\ddot{\phi} \tag{17}$$
$$\mu_b\nabla^2\psi = \rho\ddot{\psi}$$

where the double dots represent partial differentiation with respect to time. Assuming monochromatic solutions for the potentials[33] one can arrive at the following longitudinal and shear wave velocities

$$c_l = \sqrt{\frac{H}{\rho}} \tag{18}$$
$$c_s = \sqrt{\frac{\mu_b}{\rho}}$$

Substitution of the expression for H (Ref. 32) gives our desired results

$$c_l = \sqrt{\frac{[(K_r-K_b)^2/(K_r(1+\beta(K_r/K_f-1))-K_b)] + K_b + 4\mu_b/3}{\beta\rho_f + (1-\beta)\rho_s}} \tag{19}$$

$$c_s = \sqrt{\frac{\mu_b}{\beta\rho_f + (1-\beta)\rho_s}} \tag{20}$$

In this expression, in addition to previously defined quantities, K_r is the bulk modulus of the saline ice in the limit as β goes to zero , K_f is the bulk modulus of the pore brine, and K_b is the bulk modulus of the ice frame. The parameters K_r and K_b allow introduction of frame properties unique from the inherent properties of nonsaline ice, and the pore brine. These are important degrees of freedom which avoid treating saline ice as simply freshwater ice with holes drilled in it. It is not apparent that this type of freedom is built into the theoretical results of Ref.2.

Comparison of Eqs 19 and 20 with Eqs. 5 and 6 shows that

$$\mu^{eff}_i = \mu_b \tag{21}$$

$$K^{eff}_i = \left[\frac{(K_r - K_b)^2}{(K_r(1+\beta(K_r/K_f - 1)) - K_b)}\right] + K_b. \tag{22}$$

Clay and Medwin[34] have derived an expression equivalent to Eq. 22 via a different method.

The results above indicate that seven parameters are needed to characterize a closed-pore, air-free Biot solid i.e. β, ρ_s, ρ_f, μ_b, K_b, K_r, and K_f, all of which are easily interpreted physically. Equation 8 is a direct determination of the Biot parameter μ_b. The experimentally determined effective bulk modulus can be used to determine K_b using Eq. 22. Solving Eq. 22 for K_b gives

$$K_b = K_r\left[\frac{\beta K^{eff}_i(K_r - K_f) - K_f(K_r - K^{eff}_i)}{\beta K_r(K_r - K_f) - K_f(K_r - K^{eff}_i)}\right] \tag{23}$$

Equation 23 shows that, in addition to the experimentally determined values of K^{eff}_i and K_r from (K^{eff}_i at β=0), one needs a value for K_f to obtain K_b. We assumed $K_f = 2.07\times10^9$ Nt/m^2 ; a value which corresponds to an acoustic velocity of about 1440 m/sec which is typical for arctic

sea water at its freezing temperature

C. Calculation of Biot Moduli

Examination of Eqs. 7, 8, 12-14, 21, and 23 reveals that the Biot frame moduli μ_b and K_b have a T dependence in addition to that accounted for by the porosity. In the present analysis this additional dependence is entirely due to the temperature dependence of ρ_s and ρ_f since the velocities were assumed to be functions of porosity only. Additional dependence on S and T separately would seem possible. For instance, saline ice with S=4 ppt, T=-3°C and saline ice with S= 10 ppt, T=-9°C would both have porosities of about 6.3 percent, but it is easy believe the frame rigidity could be different in the two cases. Furthermore, varying histories might easily cause ice with the same S,T to have different frame rigidity. These realities could be in part responsible for the scatter of data in Fig. 2 but examination of these issues is beyond the scope of the present effort.

As an indication of the magnitude of the additional dependence, K_b is plotted in Fig. 3 as a function of porosity for ice of several different salinities. The temperature range for all curves was -2 to -30 degrees. In the figure we have set a lower physical limit of zero on the modulus.

Having progressed from in-field measurement to Biot moduli we now change orientation. The fundamental physical parameters of ice, as modeled here, are taken to be β, ρ_s, ρ_f, μ_b, K_b, K_r,and K_f. Quantities such as the effective moduli and the velocities are derivable from these parameters using Eqs. 19-22. An important result is that it is the physical limits on these fundamental parameters which must not be violated. Thus Eq. 8,9, and 23 are to be used to predict the Biot moduli until the lower physical limit of zero is reached. A useful consistency check is possible at the lower limit on K_b, and μ_b. When the frame moduli equal zero Eqn. 19 should be that of suspension theory of unconsolidated mixtures. That this indeed the case can be seen using the suspension theory results in Ref. 35.

At this point our development is complete. A model of sea ice has been developed and the physical parameters of the model determined from experiment. Acoustic velocities for ice can be predicted from knowledge of the salinity and temperature of the ice and use of Eqs. 7,8,11-14 and 23. If one incorporates the zero limits on the Biot moduli, calculation for all porosities between zero and one are possible. (As discussed above the actual porosities typically seen in nature are $0 \leq \beta \leq 0.25$.) Table I, giving example values, is included as an aid to implementation of these relations.

IV. APPLICATIONS

In this section we apply the above results. First, we an examine the acoustic effects of cycling an ice core through a range of temperatures. Then, we calculate average vertical velocities through the ice canopy for different thicknesses and air/ice surface temperatures.

A. Effects of Temperature Cycling

One of the original motivations of the experimental technique was to minimize deviation of the ice temperature from its in-situ value. The question of temperature effects on acoustic properties motivated us to perform an experiment during APLIS 90 in which a 7.5 cm ice core section which had an in-situ temperature of about -5.6° C was allowed to cool to environmental temperature (about -15° C) and then warmed back to its original temperature while periodically determining its acoustic veloc ities.

In this experiment the core was actually cycled through the temperature range twice. During the first cycle both longitudinal and shear wave velocities were obtained. As the core reached warm temperatures at the end of the first cycle shear coupling was lost and only longitudinal velocities obtained during the second cycle. The experimentally determined acoustic velocities found are the top curves shown in Figs. 4a and b. At the end of two temperature cycles the longitudinal velocity had changed by about 40 m/s. At the end of one temperature cycle the shear velocity

TABLE #: 1

S(ppt)	T(°C)	β (volume fraction)	ρ_w (Nt/m³)	ρ_c (Nt/m³)	K_w (Nt/m²)	K_c (Nt/m²)	μ_w (Nt/m²)	K_s (Nt/m²)	c_w (m/s)	c_i (m/s)
30	-2	.7794	917.3	1030	8.696e9	2.07e9	0	0	0	1573
30	-10	.1798	918.4	1114	8.706e9	2.07e9	1.607e9	5.559e9	1298	3057
30	-30	.0720	921.2	1252	8.733e9	2.07e9	2.552e9	7.733e9	1643	3483
10	-2	.2442	917.3	1030	8.696e9	2.07e9	1.018e9	3.950e9	1038	2772
10	-10	.0584	918.4	1114	8.706e9	2.07e9	2.631e9	7.747e9	1682	3534
10	-30	.0236	921.2	1252	8.733e9	2.07e9	2.933e9	8.430e9	1777	3659
5	-2	.1203	917.3	1030	8.696e9	2.07e9	2.090e9	6.434e9	1499	3299
5	-10	.0290	918.4	1114	8.706e9	2.07e9	2.870e9	8.247e9	1762	3639
5	-30	.0118	921.2	1252	8.733e9	2.07e9	3.024e9	8.593e9	1808	3700

had changed by about 20 m/s.

Theoretical predictions of the acoustic velocities and the changes which would be seen are the bottom curves in Fig. 4a and b. These predictions were made by using the salinity measured by melting the core at the end of the experiment and the results in Ref. 22 predicting the change in salinity during a temperature cycle. Specifically, the final salinity was 5.65 ppt, and this implies (through the equations of Ref. 22) an initial (before cycling) salinity of about 6.7 ppt if it is assumed that brine expulsion occurs during both cycles (an assumption indicated by the rise in the longitudinal wave speed in both cycles). The temperatures and predicted salinities at extreme points in the cycle were then used in the Biot results above to determine theoretical acoustic velocities. The absolute values predicted are about 3% low for the longitudinal wave and about 5% low for the shear wave, commensurate with the scatter seen in Fig. 2. The trends which occur during the cycling are well modeled by the theoretical predictions.

A notable point is that these results are for a relatively narrow temperature cycling range as compared to the type which would ensue from packing the cores in dry ice and shipping them for analysis in a laboratory.

B. Average Velocities

Of interest for low frequency efforts and ice thickness measurement are the average acoustic velocities through the ice canopy. By using a simple model for the salinity profile in first year ice and assuming a linear temperature profile from the air/ice to the ice/water interface one can determine vertical velocity profiles and subsequently average velocities using the results of Sections II and III.

Figures 5a-d shows salinity and temperature profiles (using an air/ice interface temperature ($T_{a/i}$) of -15° C) and the resulting velocity profiles for several thicknesses of ice. The salinity profiles were calculated using a simplified version of model results for first year sea ice[36,37]. The

equations, written as a function of the depth (d) below the air/ice interface and total ice thickness d_{max}, are

$$S(\text{in ppt}) \begin{cases} = 10 - 23.8(d) & 0 \le d \le 0.174\text{m} \\ = 6.0 - 0.756(d) & 0.174 < d \le 1.003\,(d_{max}) - 0.234 \\ = 9.78 - 16.2(d_{max}) + 15.4(d) & 1.003\,(d_{max}) - 0.234 < d \le d_{max}. \end{cases} \quad (24)$$

Figures 5e and f show the average velocities as a function of thickness calculated using Figs. 5c and d. The average velocities were calculated by numerical integration of the travel time through the ice canopy and division of the ice thickness by that travel time.

Of particular interest for ice thickness measurement is the average vertical longitudinal wave velocity. For this reason we have used the results of numerical integrations to derive polynomial fits for the average velocity as a function of the thickness and the ice/air interface temperature (assuming first year salinity profiles and linear temperature gradients). Figure 6a shows the average vertical longitudinal velocity as a function of ice thickness for two different air/ice surface temperatures. Figure 6b shows the average velocities as a function of air/ice surface temperature for two different thicknesses. Both the numerical integration results and polynomial fits (given below) are shown. From these results one can see that the polynomial fits can be used for thicknesses to 3m and air/ice surface temperatures to –26°C. The polynomial expressions for the average vertical longitudinal velocity, in terms of d_{max} and $T_{a/i}$, are

$$c_l^{ave} = F_1(d_{max}) + F_2(d_{max})T_{a/i} + F_3(d_{max})T_{a/i}^2 + F_4(d_{max})T_{a/i}^3 \quad (25)$$

where

$$F_1(d_{max}) = 2661.918175 + 482.513713(d_{max}) - 191.152365(d_{max})^2 + 28.11328742(d_{max})^3$$

$$F_2(d_{max}) = -134.7439813 + 62.30165590(d_{max}) - 25.70144588(d_{max})^2 + 3.82127565(d_{max})^3$$

$$F_3(d_{max}) = -7.247301576 + 3.34509833(d_{max}) - 1.38909594(d_{max})^2 + 0.206890795(d_{max})^3$$

$$F_4(d_{max}) = -0.129668213 + 0.059669323(d_{max}) - 0.024812066(d_{max})^2 + 0.003695989(d_{max})^3$$

V. SUMMARY

The obvious importance of the knowledge of the elastic parameters of sea ice to acoustic studies in the Arctic has motivated the work here. We have outlined an in-field experimental technique to determine acoustic velocities for Arctic sea ice. Using a velocity data set obtained via this method, we have determined the salinity and temperature dependence of the fundamental elastic parameters in sea ice modeled as a isotropic porous solid with closed pores. Further experimental effort is needed to increase the data base from which the elastic parameters are obtained. Further modeling effort is needed to treat cases such as multiyear ice where significant air content is possible.

A comment on inclusion of air in the porous solid model is in order. Bedford and Stern[38] have extended the Biot model to include content of a small volume of air bubbles. Their results indicate that above the resonance frequencies of the air bubbles the velocity of the longitudinal wave examined here would be essentially the same. However, below the bubble resonance frequency the velocity would be substantially depressed and at resonance the velocity goes through a maximum. The applicability of their analysis in obtaining ice acoustic velocities should be pursued.

Some of the elastic parameters obtained have been related to elastic parameters appropriate for a transversely isotropic porous solid model of the ice. Experiments in which the horizontal acoustic velocities are measured at the same time as the vertical velocities would allow determination of more of the parameters of that model.

ACKNOWLEDGEMENTS

The assistance of Dr. Pierre Mourad, Dr. Ronald Stein, and Mr. Timothy Wen in both preliminary tests of the experimental technique and in the acquisition of the data used here is gratefully acknowledged. This work was supported by the Office of Naval Technology with technical management provided by the Naval Oceanographic and Atmospheric Research Laboratory (NOARL).

APPENDIX

The data used in Fig. 2 are given here for reference. More data is needed at all porosities, but particularly the higher ones. At high porosity, shear wave coupling was difficult to establish via the method put forth in the paper. Furthermore, brine drainage effects at the higher porosities are more severe.

APPENDIX TABLE

β (vol.frac.)	c_s (m/s)	c_l (m/s)		β (vol.frac.)	c_s (m/s)	c_l (m/s)		β (vol.frac.)	c_s (m/s)	c_l (m/s)
0.004	1881	3746		0.022	1846	3730		0.026	1719	3653
0.014	1871	3727		0.022	1692	3684		0.031	1764	3572
0.015	1724	3750		0.022	1781	3626		0.031	1771	3578
0.015	1808	3520		0.022	1810	3626		0.031	1800	3597
0.015	1873	3635		0.022	1811	3686		0.033	1788	3605
0.016	1863	3713		0.022	1827	3728		0.036	1826	3706
0.018	1739	3727		0.023	1819	3694		0.037	1716	3586
0.018	1924	3642		0.023	1700	3604		0.037	1731	3396
0.019	1735	3737		0.023	1708	3722		0.039	1531	3507
0.019	1832	3741		0.023	1714	3726		0.039	1744	3505
0.019	1841	3768		0.023	1748	3624		0.044	1782	3577
0.019	1857	3708		0.023	1772	3600		0.048	1686	3443
0.020	1867	3707		0.023	1797	3692		0.059	1631	3652
0.021	1708	3710		0.024	1814	3702		0.061	1782	3653
0.021	1711	3695		0.024	1705	3714		0.072	1586	3470
0.021	1719	3713		0.024	1743	3736		0.105	1651	3176
0.021	1784	3619		0.024	1778	3559		0.154	1340	3279
0.022	1671	3481		0.025	1750	3716				

REFERENCES

1. K. L. Williams, R. Stein, T. Wen, R. E. Francois,"Determination of Elastic Moduli of Sea Ice," IEEE Oceans'89 Conference proceedings, Vol. 4, 1231-1235 (Sept. 1989).

2. C. H. Yew, X. Weng, "A Study of Reflection and Refraction of Waves at the Interface of Water and Porous Sea Ice," J. Acoust. Soc. Am. Vol 82, 342-353 (1987).

3. P. D. Mourad, K. L. Williams, "Near-normal Incidence Scattering from Rough, Finite Surfaces: Kirchhoff Theory and Data Comparison for Arctic Sea Ice," (to be submitted to J. Acoust. Soc. Am.)

4. J. H. Brown, E. E. Howick, "Physical Measurements of Sea Ice," NEL Research and Development Report 825 (U. S. Navy Electronics Laboratory, San Diego, Cal.) (1958).

5. J. H. Brown, "Elasticity and Strength of Sea Ice," In **Ice and Snow: Properties, Processes, and Applications** , edited by W. D. Kingery, Cambridge, Mass.: MIT press, 79-106 (1963).

6. D. L. Anderson, "Preliminary Results and Review of Sea Ice Elasticity and Related Studies," Trans. Eng. Inst. Canada, Vol. 2, No. 3, 116-122 (1958).

7. R. W. Boyle, D. O. Sproule, "Velocity of Longitudinal Vibration in Solid Rods (Ultrasonic Method) with Special Reference to the Elasticity of Ice," Can. J. Research, Vol. 5, No. 6, 601-618 (1931).

8. T. D. Northwood, "Sonic Determination of the Elastic Properties of Ice," Can. J. Research, Vol. 25, part A, 88-95 (1947).

9. M. P. Langleben, E. R. Pounder, "Elastic Parameters of Sea Ice," In **Ice and Snow: Properties, Processes, and Applications** , Cambridge, Mass.: MIT press, 69-78 (1963).

10. V. V. Bogorodskii, "The Elastic Characteristics of Ice," Sov. Phys. Acoust. Vol. 4, 17-21 (1958).

11. E. R. Pounder, P. Stalinsky, "General Properties of Arctic Sea Ice," Int. Assoc. of Scientific

Hydro., Publ. 54, 35-39 (1960).

12. M. P. Langleben, "Young's Modulus for Sea Ice," Can. J. Phys., Vol. 40, No. 1, 1-8 (1962).

13 V. V. Bogorodskii, "Elastic Moduli of Ice Crystals," Sov. Phys. Acoust., Vol. 10, No. 2, 124-126 (1964).

14. G. Abele, G. Frankenstein, "Snow and Ice Properties as Related to Roads and Runways in Antarctica," CRREL Report - 176 (1967).

15. H. F. Bennett, "Measurements of the Ultrasonic Wave Velocities in Ice Cores from Greenland and Antarctica," CRREL Research Report - 237, (June 1972).

16. R. E. Bunney, "Feasibility of Acoustically Determining the Thickness of Sea Ice," Appl. Phys. Lab - Univ. Wash. report 7317, (April 1974).

17. V. V. Bogorodskii, V. P. Gavrilo, A. V. Gusev, V. A. Nikitin, "Measurements of the Speed of Ultrasonic Waves in Bering Sea Ice," Sov. Phys. Acoust., Vol. 21, No. 3, 286-287 (1975).

18. V. V. Bogorodskii, V. P. Gavrilo, V. A. Nikitin, "Sound Propagation in Ice Crystallized from Salt Water," Sov. Phys. Acoust., Vol. 22, No. 2, 158-159 (1976).

19. H. Kohnen, A. J. Gow, "Ultrasonic Velocity Investigations of Crystal Anisotrophy in Deep Ice Cores from Antarctica," J. Geophys. Research, Vol 84, No. C8, 4865-4873 (1979).

20. C. H. Yew, "Use of Penetrators to Estimate the Properties of Ice in the Arctic Region," In **Proceedings of the Arctic Oceanography Conference and Workshop** , Naval Ocean Research and Development Activity, NSTL, Mississippi, 90-95 (1985).

21. P. J. Vidmar, "Synopsis of an Investigation of the Acoustical Properties of Sea Ice," Applied Research Lab. - Univ. Texas Report 87-6, Feb. 1987.

22. G. F. Cox, W. F. Weeks, "Changes in the Salinity and Porosity of Sea Ice Samples During Shipping and Storage," J. Glaciology, V. 32, 371-375 (1986).

23 M. A. Biot, "Theory of Propagation of Elastic Waves in a Fluid-Saturated Porous Solid. I.

Low-Frequency Range," J. Acoust. Soc. Am. Vol. 28, 168-178 (1956).

24 M. A. Biot, "Theory of Propagation of Elastic Waves in a Fluid-Saturated Porous Solid. II. Higher Frequency Range," J. Acoust. Soc. Am. Vol. 28, 179-191 (1956).

25. Bergdahl, "Physics of Ice and Snow as Affects Thermal Pressure,"Report series A:1, Dept. of Hydraulics, Chalmers Univ. of Tech. (1977).

26. G. R. Garrison, T. Wen, R. E. Francois, W. J. Felton, W. L. Welch, "Environmental Measurements in the Beaufort Sea, Spring 1986," Applied Physics Lab - University of Washington report 4-86 (1987)

27. J. Schwartz and W. F. Weeks, "Engineering Properties of Sea Ice," J. Glaciol. Vol. 19., pp 499-531

28 G. A. Maykut, "An Introduction to Ice in the Polar Oceans," Applied Physics Lab Report 8510 (1985).

29. G.F.N. Cox, W. F. Weeks, "Equations for Determining the Gas and Brine Volumes in Sea Ice Samples," CRREL report 82-30 (1982)

30. R. Stoll, T. Kan, "Reflection of Acoustic Waves at a Water-Sediment Interface," J. Acoust. Soc. Am. vol 70, 149-156 (1981).

31. M. A. Biot, "Mechanics of Deformation and Acoustic Propagation in Porous Media," J. Appl. Phys., vol. 33, 1482-1498 (1962).

32. R. D. Stoll, "Acoustic Waves in Saturated Sediments," in **Physics of Sound in Marine Sediments**, Ed. by L. Hampton (Plenum, New York, 1980).

33. A. L Fetter and J. D. Walecka, **Theoretical Mechanics of Particles and Continua**, chapter 13, (McGraw-Hill, New York, 1980).

34. C. S. Clay, H. Medwin, **Acoustical Oceanography: Principles and Applications**, Appendix A8, (John Wiley & Sons 1977)

35. P.L. Chambre, "Speed of a Plane Wave in a Gross Mixture," J. Acoust. Soc. Am., Vol. 26, pp. 329-331 (1954).

36. G. F. N. Cox, W. F. Weeks,"On the Profile Properties of Undeformed First Year Sea Ice," CRREL Special Report 86-30, Oct. 1986.

37. G. F. N. Cox, W. F. Weeks, "Numerical Simulation of the Profile Properties of Undeformed First-Year Sea Ice During the Growth Season," J. Geophys. Res., Vol.93, No. C10, 12,449-12,460 (1988).

38. A. Bedford, M. Stern, "A Model for Wave Propagation in gassy sediments," J. Acoust. Soc. Am. Vol 73, 409-417 (1983).

FIGURE CAPTIONS

FIG. 1. A simplified diagram of the velocity measurement apparatus is shown. The data acquisition electronics was housed in a heated work space. The sample holder as well as core preparation and monitoring equipment were outside. The experiment required the coordinated efforts of two researchers. A typical digital scope trace, after both shear and longitudinal coupling had been established, is also given.

FIG. 2. The longitudinal (c_l, data shown as open squares) and shear (c_s,data shown as open circles) velocity data obtained using the apparatus in Fig. 1. Leastsquares fit curves (equations given in text) to the data are also shown. The largest errors come in determining porosities from the salinity and temperature of the samples. This uncertainty increases with porosity (examples shown for some of the c_l data).

FIG. 3. The Biot frame modulus K_b *as function of porosity for* several assumed salinities. The results have been obtained by varying the temperature of the ice. They indicate that, besides the porosity dependence, there is an additional dependence on S and T for the model presented here. When K_b equals zero the sample would be an unconsolidated mixture and the velocity prediction of suspension theory[35] is recaptured from Eq. 19.

FIG. 4. Demonstration of the acoustic effects of temperature cycling a ice sample. Experimental results are the top connected points in each graph. The model results are the bottom connected points. Each point is numbered by its position in the cycling sequence. The model results were obtained with the aid of Ref. 22 to determine the change in porosity for a specified temperature change.

FIG. 5 Figures 5a and b show salinity and temperature profiles for several thicknesses of first year sea ice. The salinities were determined using simplified versions of model results in Ref. 36. The temperature profiles were assumed to be linear from the air/ice interface (at $-15^{\circ}C$) to the

ice/water interface (at $-2^{\circ}C$). These profiles were used to determine the longitudinal (Fig. 5c) and shear (Fig. 5d) velocity profiles for the different ice thicknesses. From the velocity profiles, average longitudinal (Fig. 5e) and shear (Fig. 5f) velocities as a function of ice thickness were obtained.

FIG. 6 Figure 6a shows the average longitudinal velocity as a function of thickness for two different air/ice surface temperatures. Figure 6b shows the average longitudinal velocity as a function of air/ce surface temperature for two ice thicknesses. The figures show results of numerical integration of the velocity profiles and polynomial fits (Eq. 25) to the integration results. They indicate the ice thickness and temperature regimes where the polynomial fits are useful.

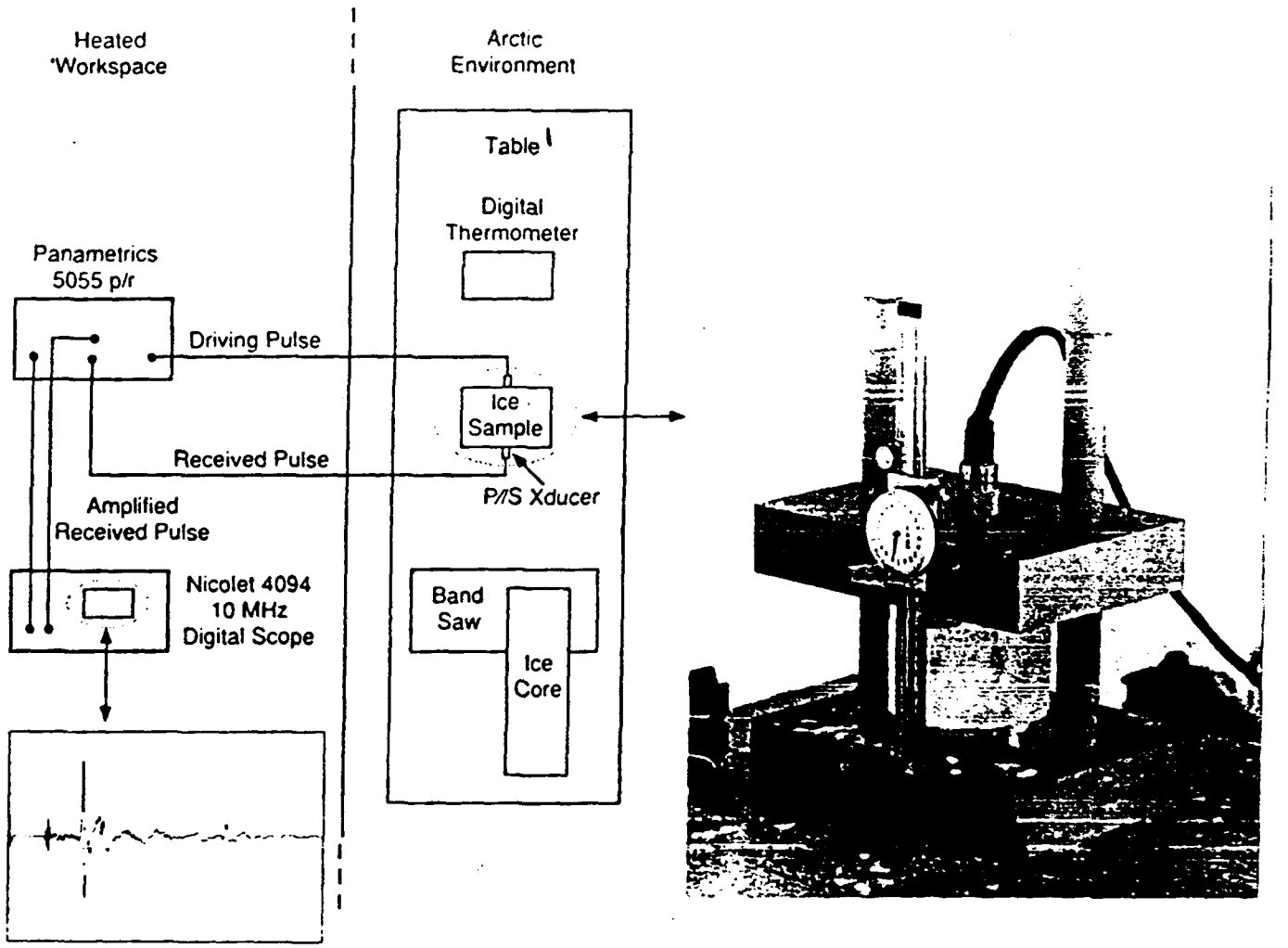
Heated
Workspace
Arctic
Environment
Table
Digital
Thermometer
Panametrics
5055 p/r
Driving Pulse
Ice
Sample
Received Pulse
P/S Xducer
Amplified
Received Pulse
Nicolet 4094
10 MHz
Digital Scope
Band
Saw
Ice
Core

Fig. 1

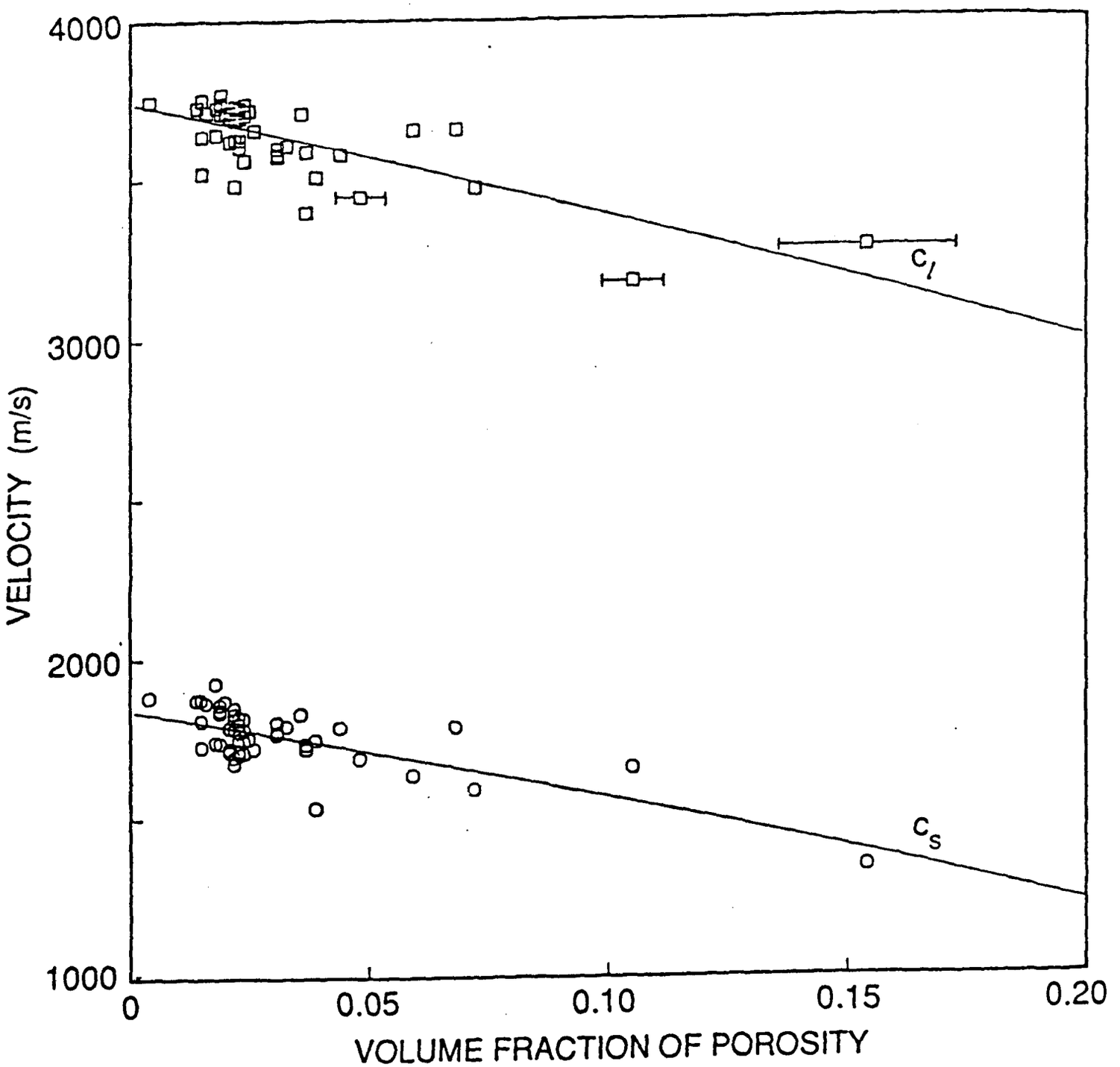
4000
3000
2000
1000
VELOCITY (m/s)
0
0.05
0.10
0.15
0.20
VOLUME FRACTION OF POROSITY
c_l
c_s

Fig. 2

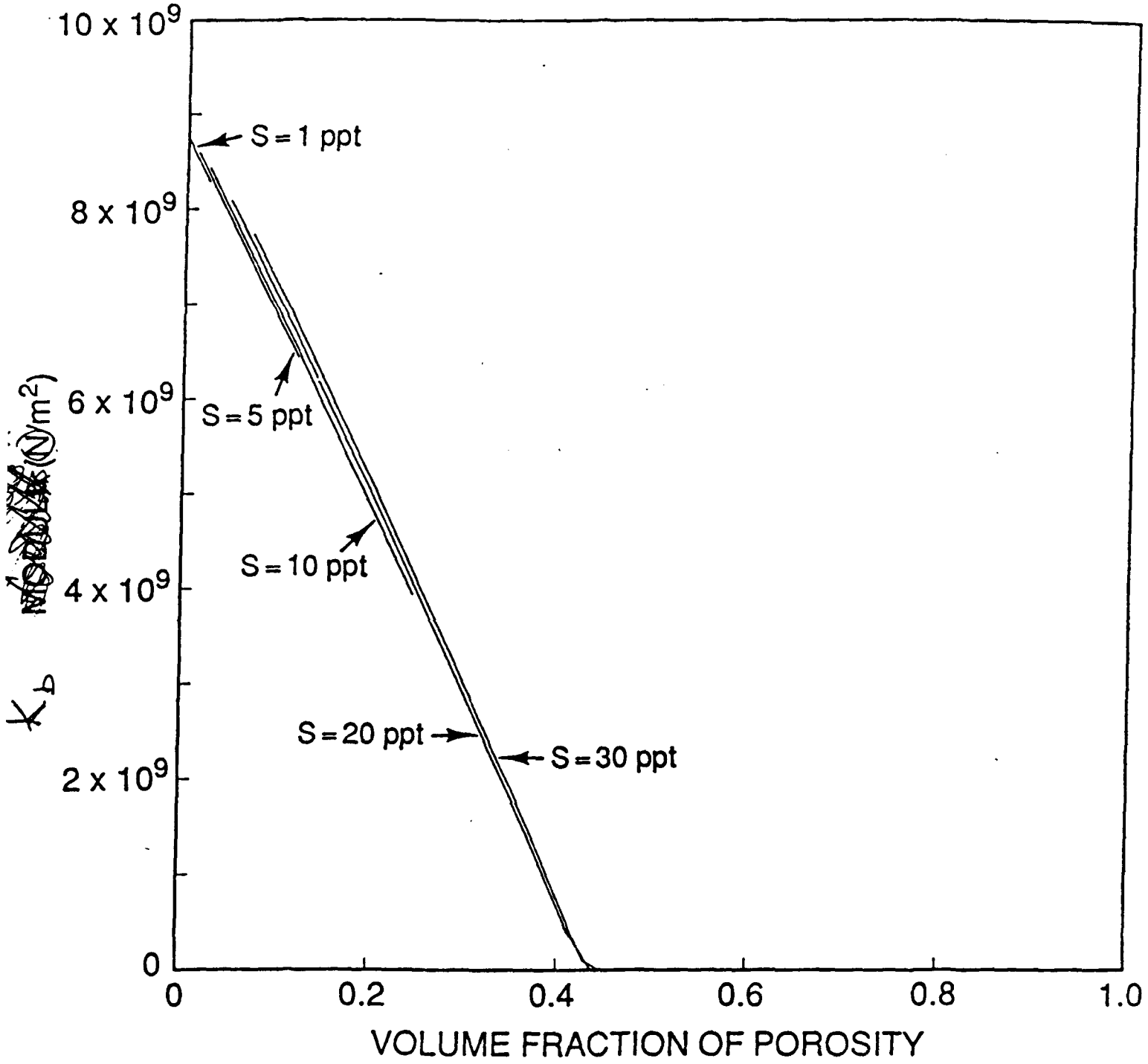
10 x 10^9
8 x 10^9
6 x 10^9
4 x 10^9
2 x 10^9
0
S = 1 ppt
S = 5 ppt
S = 10 ppt
S = 20 ppt
S = 30 ppt
0
0.2
0.4
0.6
0.8
1.0
VOLUME FRACTION OF POROSITY

Fig. 3

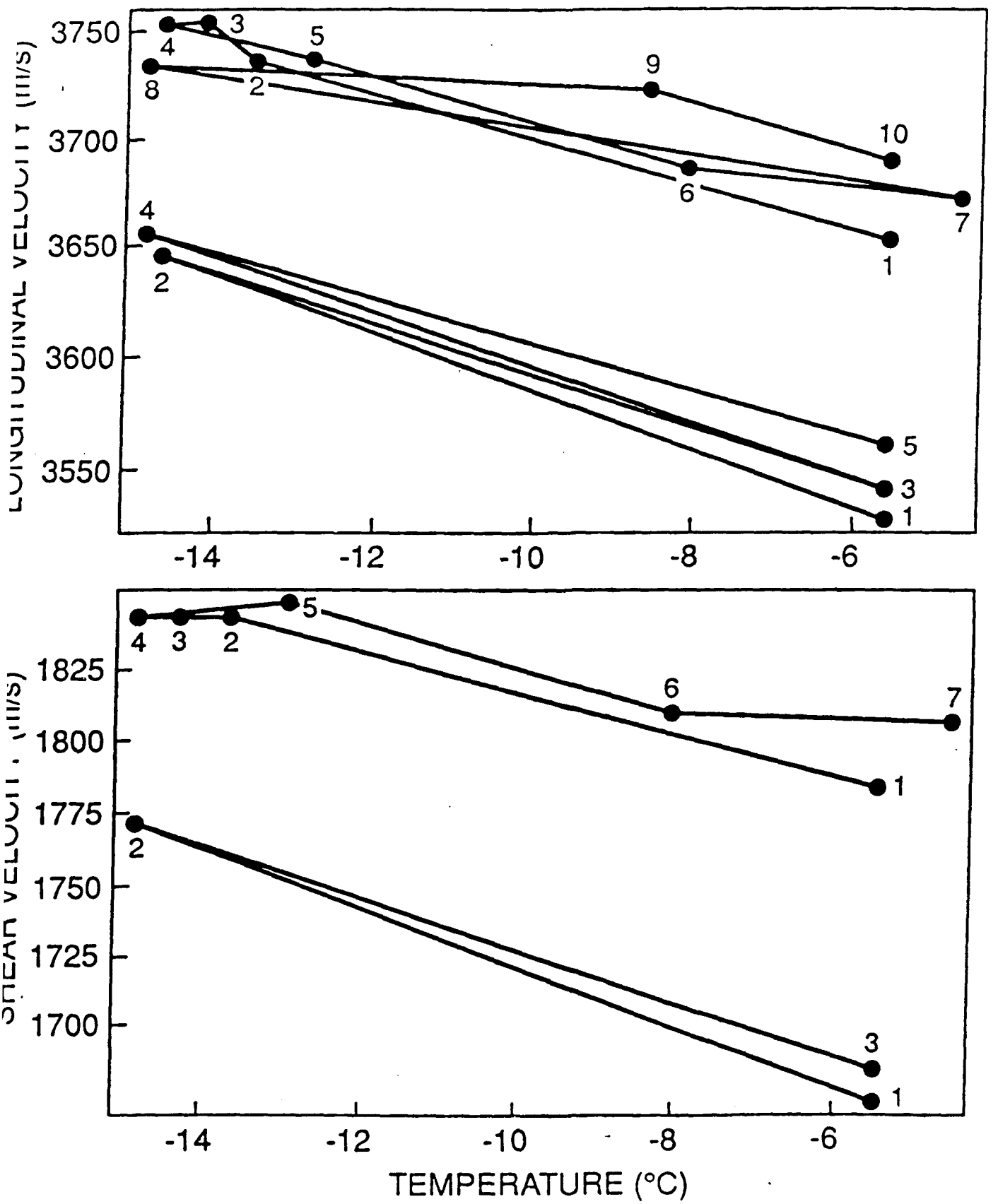
LONGITUDINAL VELOCITY (m/s)
3750
3700
3650
3600
3550
-14
-12
-10
-8
-6
SHEAR VELOCITY (m/s)
1825
1800
1775
1750
1725
1700
TEMPERATURE (°C)

Fig. 4

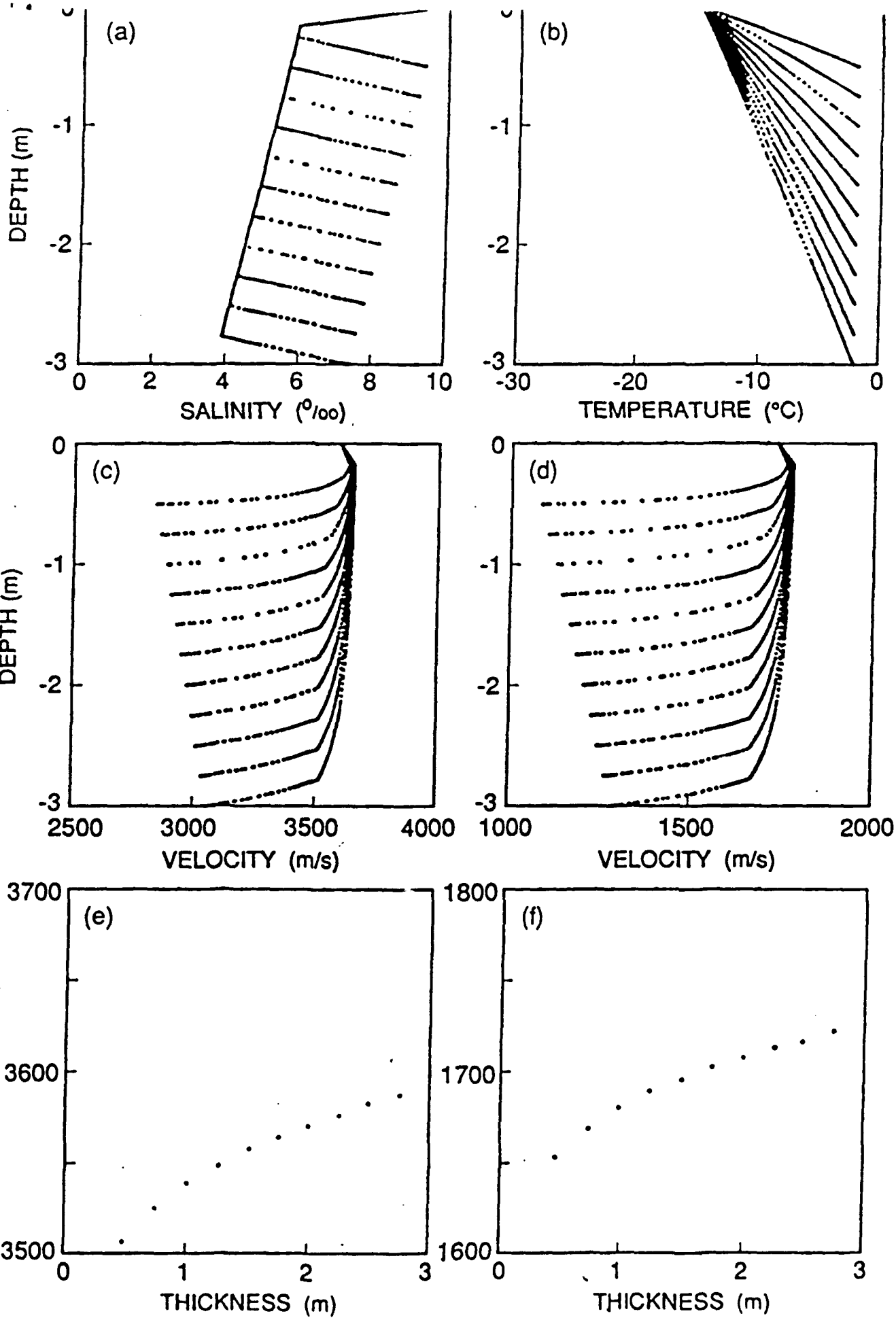
(a)
DEPTH (m)
0
-1
-2
-3
0
2
4
6
8
10
SALINITY (°/oo)
(b)
-30
-20
-10
0
TEMPERATURE (°C)
(c)
2500
3000
3500
4000
VELOCITY (m/s)
(d)
1000
1500
2000
VELOCITY (m/s)
(e)
3700
3600
3500
VELOCITY (m/s)
1
2
3
THICKNESS (m)
(f)
1800
1700
1600
THICKNESS (m)

Fig. 6

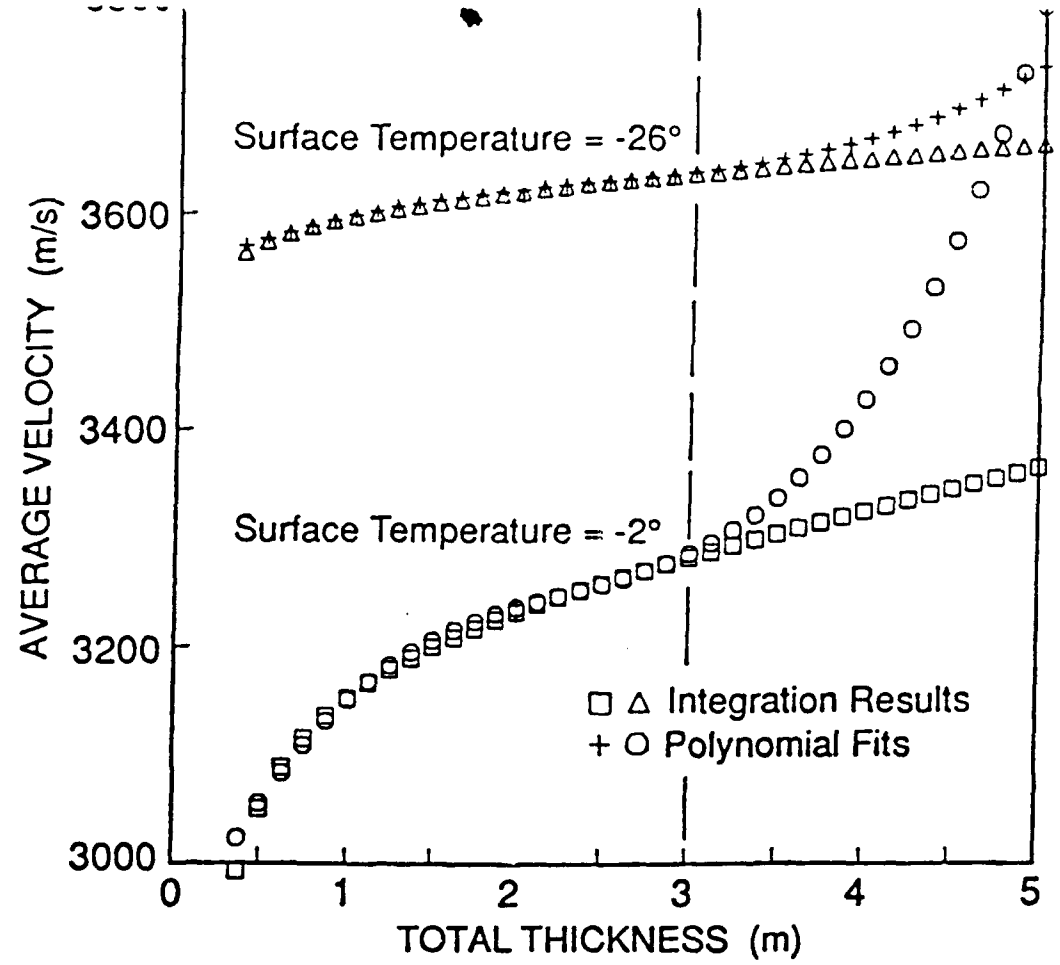
Surface Temperature = -26°
Surface Temperature = -2°
□ △ Integration Results
+ ○ Polynomial Fits
AVERAGE VELOCITY (m/s)
3000
3200
3400
3600
0
1
2
3
4
5
TOTAL THICKNESS (m)

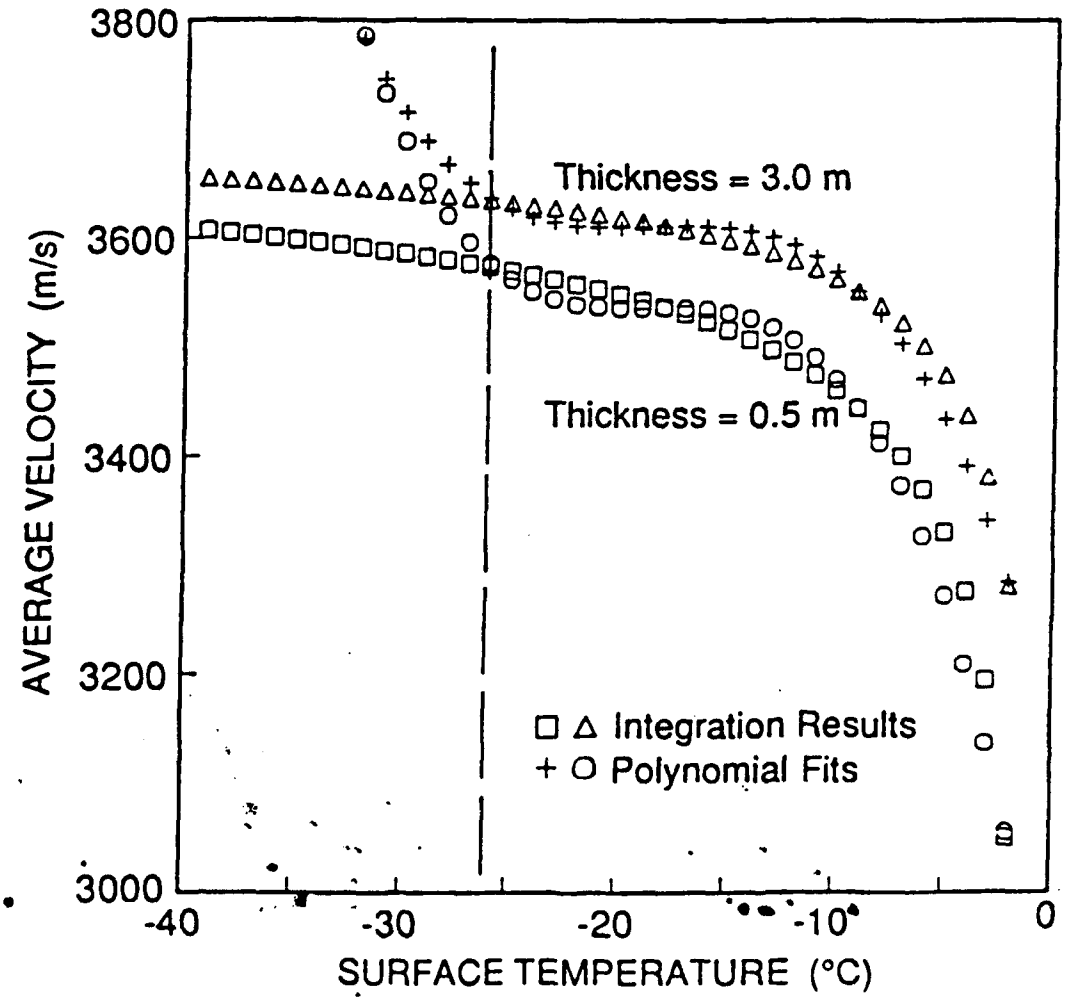
Thickness = 3.0 m
Thickness = 0.5 m
□ △ Integration Results
+ ○ Polynomial Fits
AVERAGE VELOCITY (m/s)
3000
3200
3400
3600
3800
-40
-30
-20
-10
0
SURFACE TEMPERATURE (°C)